ELASTOPLASTIC CONSTRICTION RESISTANCE OF SPHERE/FLAT CONTACTS: THEORY AND EXPERIMENT

M.R. Sridhar* and M.M. Yovanovich†

Microelectronics Heat Transfer Laboratory
Department of Mechanical Engineering
University of Waterloo
Waterloo, Ontario, Canada N2L 3G1

ABSTRACT

This paper investigates elastoplastic sphere-flat contacts from both analytical and experimental points of view. Recently, a simple elastoplastic deformation model has been proposed which is able to predict the contact radius for the three regimes of loading: elastic, elastoplastic and fully plastic. This explicit elastoplastic deformation model for circular contacts incorporated into the existing thermal constriction resistance model is used to predict the thermal constriction resistance measurements made at different load levels for sphere-flat contacts in a vacuum environment. The accuracy of prediction depends upon the value of flow stress used in the elastoplastic deformation model. Hence a technique has been proposed to calculate the appropriate value of the flow stress associated with a particular experimental set. The present model is able to predict thermal constriction resistance experimental results for a variety of metals (Keewatin Tool Steel, Nickel 200 and Carbon Steel) with an overall RMS difference of 4.5 %.

NOMENCLATURE

a	=	contact radius (m)
b	=	flux tube radius (m)
C_p	=	plastic constraint factor, = 2.76
E	=	elastic modulus (MPa)
E'	=	equivalent elastic modulus, $\equiv \left((1-\nu_1^2)/E_1 + (1-\nu_2^2)/E_2\right)^{-1}$ (MPa)
F	=	applied load (N)
F_c	=	critical load (N)
H	=	hardness (MPa)
H_B	=	bulk hardness (MPa)
k	=	thermal conductivity $W/(m \cdot K)$
k_s	=	harmonic mean thermal conductivity, $\equiv 2k_1k_2/(k_1+k_2)$ $W/(m \cdot K)$
Ni	=	Nickel
Q	=	heat transfer rate $(Watt)$
R_c	=	thermal constriction resistance (K/W)
R_c^*	=	dimensionless constriction resistance, $\equiv 2k_s b R_c$
S_f	=	material yield or flow stress (MPa)
T	=	temperature (^oC)
TS	=	Tool Steel

*Graduate Research Assistant
†Professor and Director, Fellow ASME

Greek Symbols

β	=	radius of the spherical indenter (m)
ΔT	=	effective temperature drop across the interface $(^{\circ}C)$
ψ	=	thermal constriction parameter, $\equiv (1 - a/b)^{1.5}$
ν	=	Poissons ratio
σ	=	RMS surface roughness and standard deviation of surface (m)

Subscripts

1, 2	=	sphere, flat
B	=	bulk
cT	=	constriction, theory
cE	=	constriction, experiment
e	=	elastic
ep	=	elastoplastic
p	=	plastic

INTRODUCTION

Ability to predict elastoplastic constriction resistance is of considerable interest to a thermal analyst since it enhances the contact heat transfer rate when compared to the elastic constriction resistance. Efficient heat removal is of utmost importance in thermal conduction modules with high chip densities (Fig. 1, Bar-Cohen (1987)). Each module has an array of chips mounted on the surface. Heat generated within a single chip is removed through a spring loaded piston assembly which is in contact with the chip surface. There can be many ways by which the heat removal rate could be enhanced. One way is to add an expensive thermally conductive layer to the piston/chip interface. Another way would be to load the interface such that the deformation mode moves into the elastoplastic or the fully plastic regime.

In a typical piston/chip interface contact heat transfer occurs both through the solid contact as well as the gap. Heat transfer through natural convection and radiation across the gap has been found to be negligible from previous studies. It is also known that the coupling between solid conduction and gap conduction at the contact is weak. To simplify the analysis heat transfer across the gap is neglected. This is achieved experimentally by working in a vacuum environment. Hence this study will examine a single piston/chip contact at different loads in vacuum (i.e. only solid heat transfer).

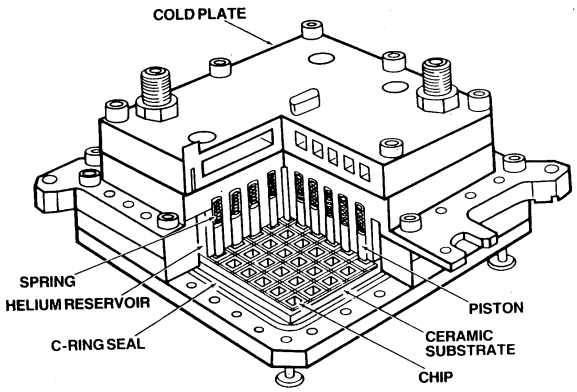

Fig.1 Thermal conduction module

The purpose of this paper is to develop a model to predict accurately the constriction resistances for interfaces which have been loaded beyond the elastic regime, i.e. to the elastoplastic and fully plastic regimes.

REVIEW OF CONSTRICTION RESISTANCE MODEL

In the complete model (Fig. 2) the contacting bodies are assumed to be smooth or with negligible roughness. It is also assumed that heat flowing between idealised bodies must flow through the solid contact area. The constriction and the subsequent spreading of heat flow lines give rise to thermal constriction resistance defined as the temperature difference across the contact divided by the total heat flow rate through the contact.

The constriction resistance model can be divided into two parts:

i) Thermal Model

Figure 2a shows the thermal model. The piston is modelled as an insulated cylindrical flux tube of radius b with a spherical cap and the chip as another insulated cylindrical flux tube of the same radius with a flat end. The problem involving two cylinders can be further reduced to a simpler problem of one cylinder with temperature specified over part of the boundary (the contact area) and zero heat flux specified over the remainder.

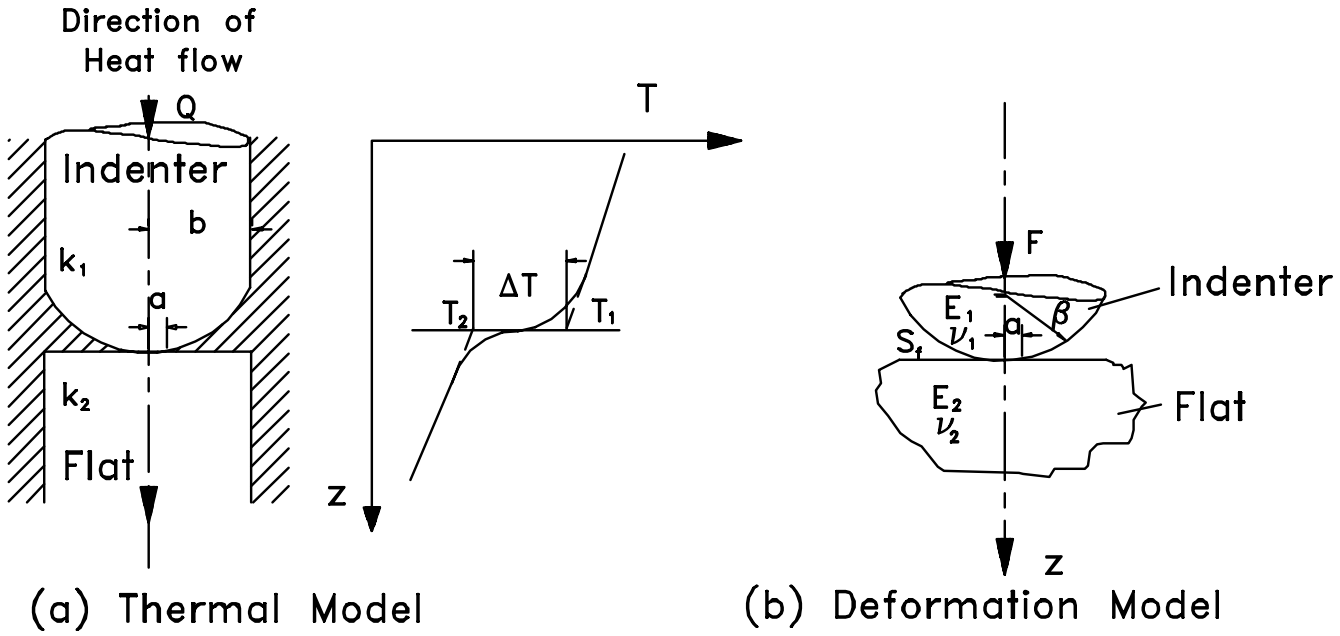

Fig.2 Thermal and deformation models of contact

The thermal constriction resistance for a circular contact spot on a flux tube has been theoretically determined by Roess and Mikic independently (see Cooper, Mikic and Yovanovich (1969)). For a circular contact spot radius, a, on a material of flux tube radius, b, we have (see Fig. 2a):

$$R_c = \frac{\psi}{4ka} \tag{1}$$

The constriction parameter depends upon the flux distribution imposed on the contact spot and the contact spot geometry. The approximate constriction parameter ψ for an equivalent isothermal contact is given by (Cooper, Mikic and Yovanovich (1969)):

$$\psi = \left(1 - \frac{a}{b}\right)^{1.5} \tag{2}$$

where a and b are the contact and flux tube radii respectively.

For a sphere-flat contact, the contact resistance is the sum of two constriction resistances:

$$R_{cT} = \frac{\psi}{4k_1 a} + \frac{\psi}{4k_2 a} = \frac{(1 - a/b)^{1.5}}{2k_s a} \tag{3}$$

where k_s is harmonic mean thermal conductivity given by:

$$k_s = \frac{2k_1 k_2}{k_1 + k_2} \tag{4}$$

The constriction resistance model, Eq. (3), requires a deformation model to predict the circular contact radius a. Once the contact radius has been predicted by the deformation model, Eq. (3) can be used to predict the thermal contact resistance.

ii) Deformation model

Figure 2b shows the deformation model. The piston is modelled as a spherical indenter with radius β and the chip is modelled as the flat. The contact deformation can be elastic, elastoplastic or fully plastic depending upon the normal load F applied. Three types of deformation models are available in the literature.

1. Elastic model of Hertz

A sphere in contact with a flat produces a circular contact. Hertz solved the problem for an elliptical contact. The circular contact is a special case of the elliptical contact problem. He simplified the problem by assuming that each body can be regarded as an elastic half space loaded over a small elliptical or circular (in this case) region of its plane surface. The Hertz contact radius "a" in terms of load F, geometry β and equivalent elastic modulus E' is given by (see Johnson (1985)):

$$a_e = \left(\frac{3F\beta}{4E'}\right)^{1/3} \tag{5}$$

where $\beta \equiv$ radius of the sphere, and the equivalent elastic modulus (E'):

$$E' = \left(\frac{1-\nu_1^2}{E_1} + \frac{1-\nu_2^2}{E_2}\right)^{-1}$$

2. Geometric Plastic model

This model assumes that the sphere and the flat interact geometrically under fully plastic deformation. Hence the contact radius in terms of load F and uniaxial tensile flow stress S_f of the softer material in contact is given by:

$$a_p = \left(\frac{F}{C_p \pi S_f}\right)^{1/2} \tag{6}$$

where

$C_p \equiv \dfrac{H}{S_f} = 2.76$, plastic constraint factor (Sridhar and Yovanovich (1993))

$H \equiv \dfrac{F}{\pi a_p^2}$, Normal indentation hardness

The ratio of hardness H, to the flow stress S_f under fully plastic deformation is a constant for real strain hardening materials provided the appropriate value of flow stress S_f is used (see Tabor (1951)).

The Hertz elastic and the geometric plastic models are inadequate to predict experimental results which lie in the elastoplastic regime.

3. Elastoplastic Model

Recently Sridhar and Yovanovich (1993) have proposed an explicit elastoplastic model by blending the two asymptotic results from the Hertz elastic model and the geometric plastic model. This simple model is able to predict experimental results for all three regimes of loading namely, the elastic, the elastoplastic and the fully plastic. It is in the form of an explicit expression and in dimensionless form it is given by:

$$\left(\frac{a}{\beta}\right)_{ep} = \left[\left(\frac{a}{\beta}\right)_e^n + \left(\frac{a}{\beta}\right)_p^n\right]^{1/n} \tag{7}$$

Substituting Eq. (5) and Eq. (6) in Eq. (7) gives

$$\left(\frac{a}{\beta}\right)_{ep} = \left[\left(\frac{3F}{4\beta^2 E'}\right)^{n/3} + \left(\frac{F}{2.76\pi\beta^2 S_f}\right)^{n/2}\right]^{1/n} \tag{8}$$

The index 'n' is called the *blending* parameter. It is to be determined from analysis, experimental results or numerical results. In this case 'n' was determined (see Sridhar and Yovanovich (1993)) by matching the predictions of Eq. (8) against accurate indentation data obtained by Tabor (1951). It was found with $n = 5$, Eq. (8) predicts values which are in excellent agreement with experimental data.

The first term on the right had side of the above Eq. (8) is the elastic solution and the second term is the fully plastic solution. They both depend on the normal load F and sphere radius β but to different powers, i.e. $n/3$ and $n/2$ for elastic and plastic limits respectively. At initial loading the first term is considerably greater than the second one. But the two approach each other as the load is increased. When the load is considerably large, the elastic term is negligible relative to the plastic term.

The above statement can be explained using a technique developed by Archard (1980). This simple technique is used to estimate the load ranges for elastic and plastic contact behavior. The ranges of fully elastic and fully plastic behavior are defined in terms of a critical load F_c, where the elastic and plastic theories predict the same value for the contact radius:

$$F_c = 366.7 \left(\frac{S_f}{E'}\right)^2 \beta^2 \, S_f \tag{9}$$

Table 1 shows how the elastoplastic model behaves under different load ranges. The load ranges presented here are slightly different from what Archard (1980) had recommended (see Sridhar and Yovanovich (1993)).

The proposed model goes smoothly to the elastic solution $F \leq 0.05\ F_c$ and goes to the fully plastic solution for $F \geq 20\ F_c$, and provides an accurate approximate solution for the intermediate elastoplastic regime defined by the load range $0.05 \leq F/F_c \leq 20$.

REVIEW OF EXPERIMENTS

Previously performed thermal contact resistance experiments of Kitscha (1982), Fisher (1985) and Fisher and Yovanovich (1989) will be utilised for comparison with theoretical predictions.

Apparatus and Procedure

i) Fisher (1985), Fisher and Yovanovich (1989)

Experiments which were performed on Ni200, and Keewatin TS flats. The indenter was made of Carbon Steel. The specimens were ground and lapped smooth. This permitted one to neglect surface roughness effects.

Table 1 Behavior of the elastoplastic model at different load levels

Deformation	Load Range	Elastoplastic model
Fully Elastic	$F \leq 0.05\ F_c$	$\left(\frac{a}{\beta}\right)_{ep} \simeq \left(\frac{a}{\beta}\right)_{e} = \left(\frac{3F}{4\beta^2 E'}\right)^{1/3}$
Elastoplastic	$0.05\ F_c \leq \mathrm{F} \leq 20 F_c$	$\left(\frac{a}{\beta}\right)_{ep} = \left[\left(\frac{3F}{4\beta^2 E'}\right)^{n/3} + \left(\frac{F}{2.76\pi\beta^2 S_f}\right)^{n/2}\right]^{1/n}$
Fully Plastic	$F \geq 20\ F_c$	$\left(\frac{a}{\beta}\right)_{ep} \simeq \left(\frac{a}{\beta}\right)_{p} = \left(\frac{F}{2.76\pi\beta^2 S_f}\right)^{1/2}$

The properties of the flat specimens and steel spheres are listed in Table 2 which were obtained from Fisher (1985) and Fisher and Yovanovich (1989). Axial loads were applied directly to the test column by a dead weight loading system. Heat was supplied to the column by a pair of resistive cartridge heaters positioned within the source specimen. The heat which flowed axially downward was removed by a cold water bath (heat sink). The column was wrapped in insulation to reduce heat losses. In order to minimize convective and conductive heat transfer across the gap, tests were conducted in vacuum (less than 1×10^{-5} torr).

ii) Kitscha (1982)

Both the ball indenter and the flat were made of Steel (see Table 3). The flat was surface-ground, then polished with fine sandpaper to produce a surface roughness of 0.127 μm (RMS). The properties of the flat specimen and Steel indenter are listed in Table 3 which was obtained from Kitscha (1982). The gas pressure was controlled by a mechanical pump and diffusion pump. The heat input to the sytem was accomplished by an electrical heating element placed in the source sample and a controlled water bath heat removal system on the sink side. A calibrated load cell determined the load on the specimens. The entire test assembly was insulated by 0.0125 m thick urethane insulation and encased in aluminum foil to minimize heat losses by radiation and convection to the surrondings. Tests were conducted in vacuum (1×10^{-5} torr).

The experimental contact resistance R_{cE} was defined as the temperature difference ΔT across the contact divided by the heat flow rate Q through the contact:

$$R_{cE} = \frac{\Delta T}{Q} \tag{10}$$

where

$$\Delta T = T_1 - T_2 \tag{11}$$

The contact temperature drop ΔT was the difference in the extrapolated average contact plane temperatures, T_1 and T_2, where T_1 and T_2 correspond to sphere and test specimen respectively (Fig. 2a).

RESULTS AND DISCUSSION

Equation (3) and Eq. (8) constitutes a complete elastoplastic constriction resistance model. Most of the thermophysical (k_s, E') and geometric parameters (β, b) are known before hand and are constants for a particular experimental set. The only unknown parameter is the uniaxial tensile flow stress S_f.

It is clear from Tabor's work (1951) that flow stress "S_f" is not a constant for a real strain hardening material; it varies with increasing contact strain under plastic deformation. In the present set of experiments uniaxial tensile flow stress S_f is not available. Fisher and Yovanovich (1989) calculated the flow stress from a bulk hardness test using Tabor's (1951) empirical relationship between hardness and flow stress given by:

Table 2 Properties of specimens of Fisher (1985) and Fisher and Yovanovich (1989)

Specimens	Material	β m	b m	E MPa	ν	k $W/(m \cdot K)$	σ μm
Flat1	Ni200	∞	0.0125	204000	0.3	79.3	0.12
Flat2	Ni200	∞	0.0125	204000	0.3	79.3	0.12
Flat3	Ni200	∞	0.0125	204000	0.3	79.3	0.06
Flat4	Keewatin TS	∞	0.0125	204000	0.3	33.5	< 0.05
Indenter1	Carbon Steel	0.01905	0.0125	207000	0.3	45.7	—-
Indenter2	Carbon Steel	0.03810	0.0125	207000	0.3	45.7	< 0.05

Table 3 Properties of specimens of Kitscha (1982)

Specimens	Material	β m	b m	E MPa	ν	k $W/(m \cdot K)$	σ μm
Flat5	1020 Steel	∞	0.0125	207000	0.3	52.8	0.127
Indenter3	Carbon Steel	0.0125	0.0125	207000	0.3	50.2	—

$$S_f = \frac{H_B}{C_p} \tag{12}$$

where $H_B \equiv$ bulk hardness.

This is a good approximation provided both the bulk hardness test and experiments are performed approximately at the same contact strain (a/β). But this is not possible for the present set of experiments. To avoid the problem of not using an appropriate value of flow stress, a technique was developed to calculate S_f. The present method assumes that the flow stress S_f is a constant for a particular experimental set. This is a reasonable assumption since most of the present experimental data lie in the elastic and the elastoplastic regimes. Hence, the value of flow stress which is a constant for an experimental set would be more or less close to the yield stress of the softer material in contact.

Procedure to calculate appropriate flow stress S_f

The method is illustrated with the help of the flow chart shown in Fig. 3. The first step would be to input values of experimental resistance R_{cE} (at maximum load F_{max}), harmonic mean thermal conductivity k_s, equivalent elastic modulus E' and geometric properties b and β for a particular data set. With this information the contact radius can be calculated solving Eq. (3) using *Mathematica*[1] or any other numerical root finding technique. It should be noted that the theoretical resistance R_{cT} in Eq. (3) is replaced with the experimental value R_{cE} at F_{max}. Then the contact strain (a/β) at F_{max} for that data set can be computed. This contact

[1] Wolfram (1988, 1991)

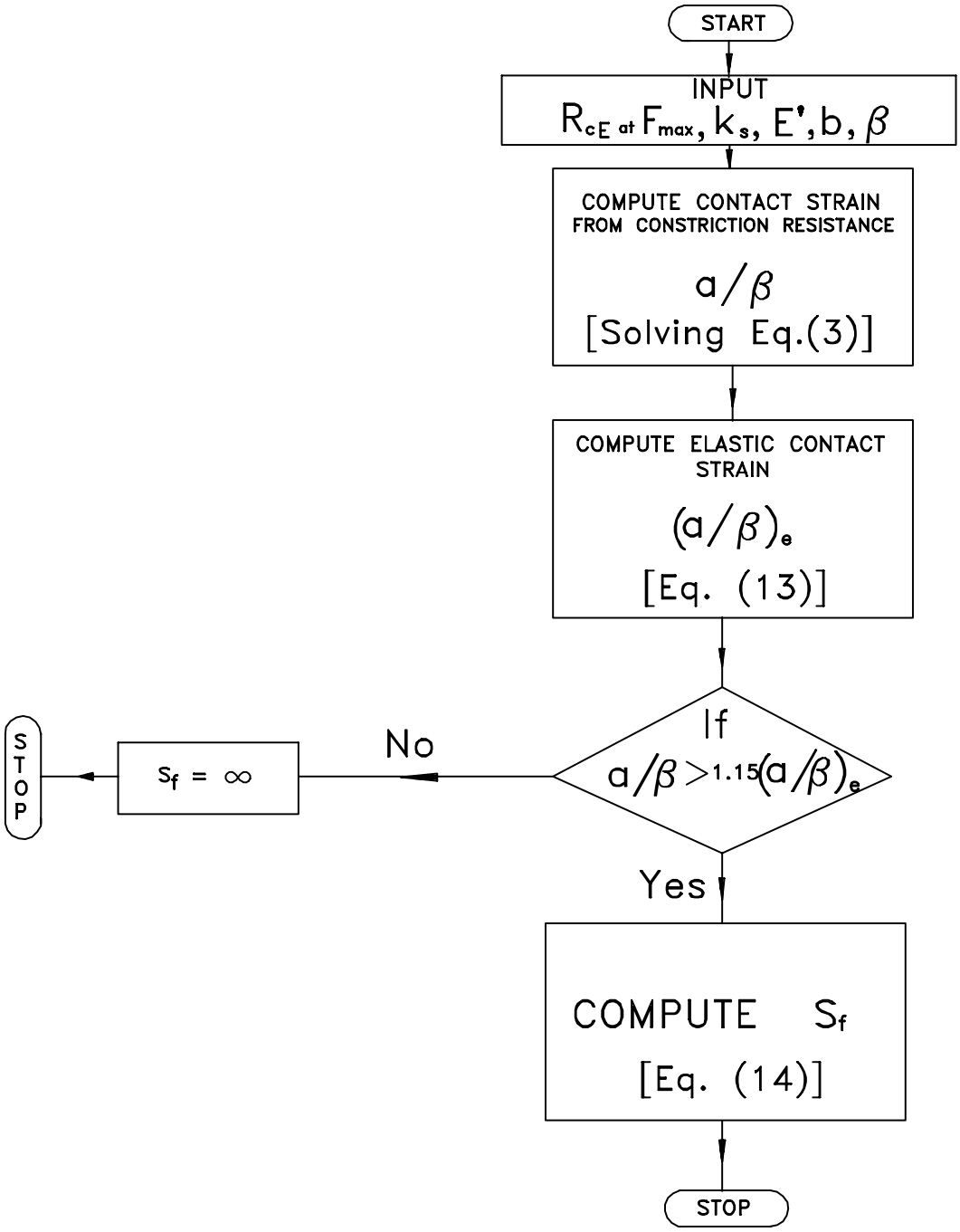

Fig.3 Procedure to calculate appropriate flow stress S_f

strain can either be in the elastic, elastoplastic or fully plastic regimes. In order to predict a realistic value of S_f one must make sure that a significant amount of plastic deformation has occurred at this particular load F_{max}. To confirm this the contact strain calculated from the experimental constriction resistance is than compared with the contact strain predicted by the Hertz elastic model given by:

$$\left(\frac{a}{\beta}\right)_e = \left(\frac{3F}{4\beta^2 E'}\right)^{1/3} \tag{13}$$

It should also be confirmed that the calculated value of contact strain should be outside the experimental uncertainity of elastic deformation since it is predicted from an experimental constriction resistance. This is done in the flow chart by comparing the computed contact strain (a/β) with 1.15 $(a/\beta)_e$ instead of just $(a/\beta)_e$. The factor 1.15 is used since the uncertainity of the computed contact strain (a/β) is of the order of $\pm$ 13.4 %. This is the root mean square of the uncertainties in the experimental resistance R_{cE} ($\pm$ 8 %), harmonic mean conductivity k_s ($\pm$ 4 %) and the radius of curvature β ($\pm$ 10 %). If the calculated value of contact strain is greater than 1.15 $(a/\beta)_e$, then the flow stress of the softer material in contact can be determined using the following relationship:

$$S_f = \frac{F_{max}}{2.76\pi\beta^2\left[\left(\frac{a}{\beta}\right)_{ep}^{n} - \left(\frac{3F_{max}}{4\beta^2 E'}\right)^{n/3}\right]^{2/n}} \tag{14}$$

If the calculated value of contact strain is less than 1.15 $(a/\beta)_e$ then the procedure recommends using a value of ∞ for the flow stress S_f. This value of flow stress reduces the elastoplastic model to the Hertz elastic model, Eq. (13).

Comparison of elastoplastic model with experiments

Figure 4 shows a comparison between data set F1 and the elastoplastic model. The asymptotic models, namely the Hertz elastic model and the geometric plastic model, have been included. It can be seen that the elastoplastic model moves smoothly from the elastic to the plastic asymptote. Experimental set F1 is a combination of Indenter1-Flat1 (Table 2). Experimental data for this set have been obtained at loads ranging from 24 N to 688 N. The value of flow stress predicted using the above procedure (Fig. 3) at a maximum load F_{max} of 688 N was 206 *MPa*. With this value of flow stress the elastoplastic constriction model, Eq. (3) and Eq. (8), is able to predict data set F1 quite well with a maximum error and RMS error of 4.2% and 2.4% respectively.

Figure 5 shows comparisons between data sets F2 and F3 with the elastoplastic constriction model. Experimental set F2 is a combination of Indenter2 and Flat2 (Table 2). The flow stress predicted for set F2 using the procedure (Fig. 3) was 194 *MPa*. Again the elastoplastic model does a good job of predicting the results with a maximum error and RMS error of 8.3% and 5.5% respectively. Experimental set F3 is similar to F2. F3 is a combination of Indenter2 and Flat3. The only difference between F3 and F2 is that Flat3 has a lower surface roughness σ (see Table 2). The procedure predicts a value of ∞ for the flow stress, which shows that the deformation is predominantly elastic for set F3. This is because the value of contact strain computed solving Eq. (3) is well within the experimental uncertainity of prediction of the elastic model. This data set compares quite well with the reduced elastoplastic model (i.e. elastic model) with a maximum error and RMS error of -8.5% and 6.1% respectively.

Figures 6 and 7 show the comparisons of data sets F4 and K1 respectively with the reduced elastoplastic model (i.e. elastic model). F4 is a combination of Indenter2 and Flat4 (Table 2) and K1 is a combination of Indenter3 and Flat5. Comparisons between data sets and reduced elastic model are excellent with RMS errors of 3.1% and 3.9% respectively.

Table 4 summarises the flow stresses, maximum and RMS errors for all data sets used in this study.

In the previous work of Fisher (1985), Fisher and Yovanovich (1989) and Kitscha (1982) the half space thermal constriction resistance model was used. Hence the constriction parameter in Eq. (3) was:

$$\psi = 1.0 \tag{15}$$

The merit of using a flux tube thermal constriction resistance model instead of a half space model can be seen by comparing the last two columns of Table 4 where % RMS errors are listed for all data sets used in the present investigation with and without the constriction parameter. It should be noted that the constriction parameter becomes increasingly important at higher loads.

The dimensionless contact resistance can be defined as:

$$R_c^* = 2bk_sR_c = \frac{(1-a/b)^{1.5}}{a/b} \tag{16}$$

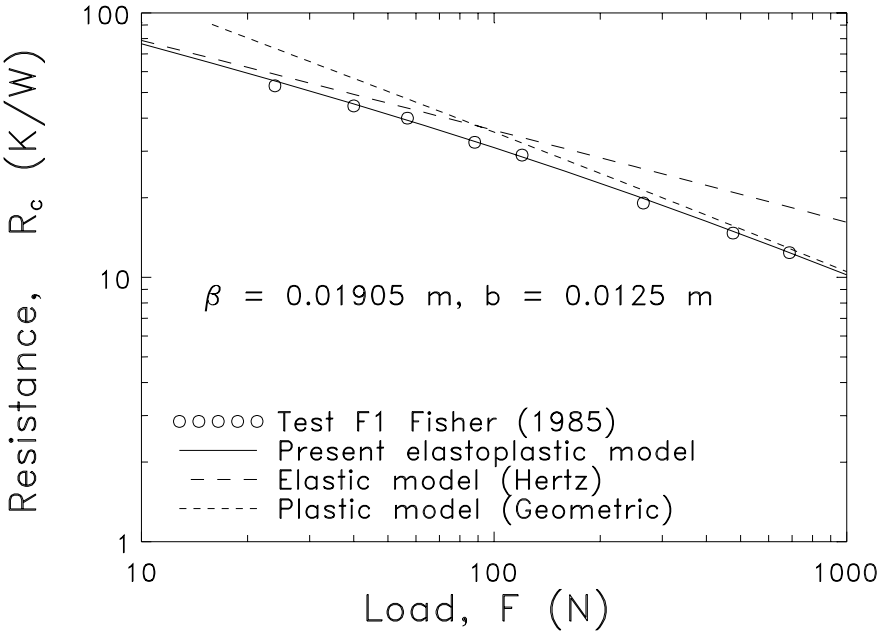

Fig.4 Constriction resistance versus load for data set F1

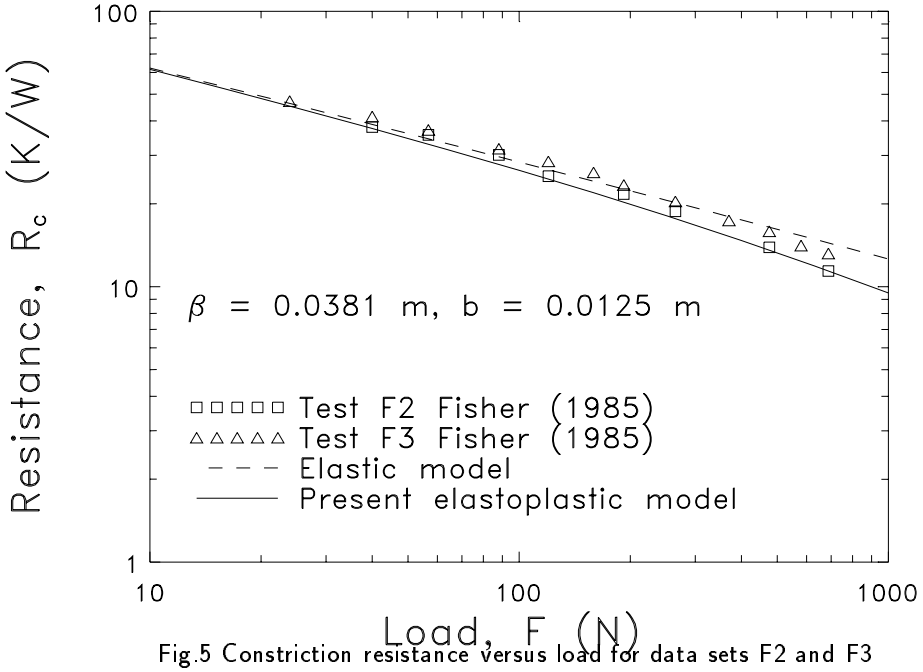

Fig.5 Constriction resistance versus load for data sets F2 and F3

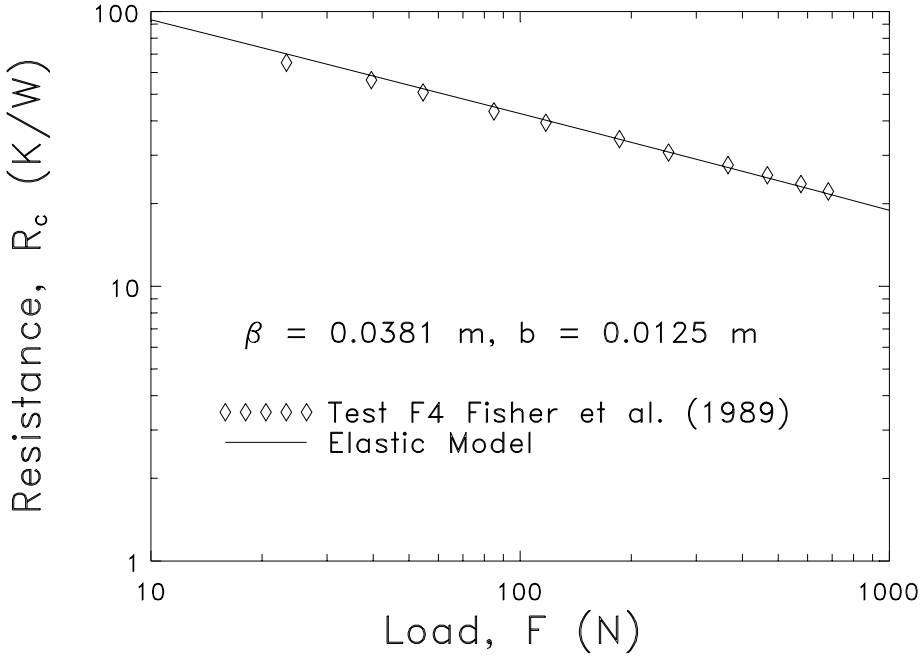

Fig.6 Constriction resistance versus load for data set F4

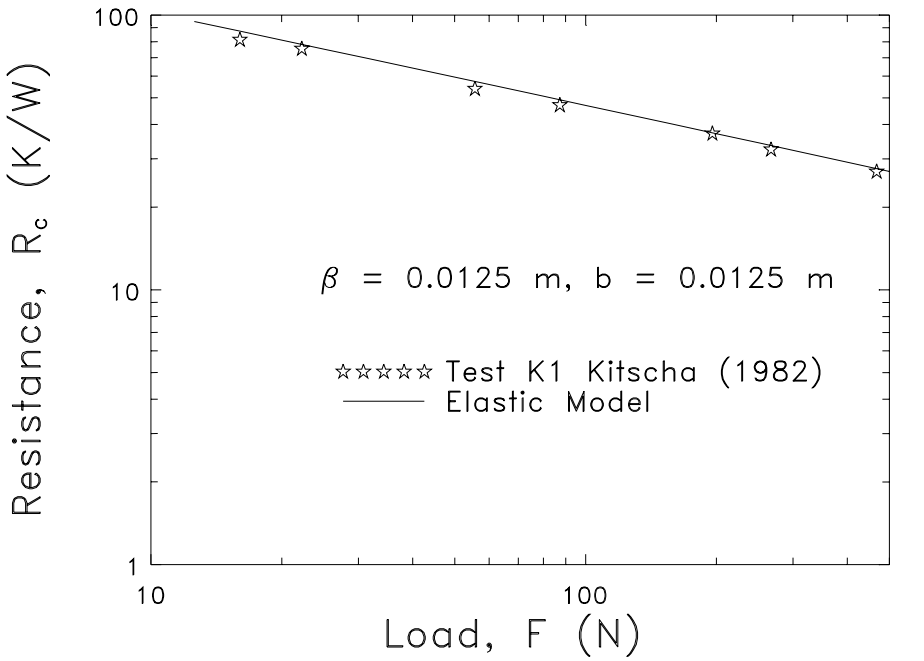

Fig.7 Constriction resistance versus load for data set K1

Table 4 Comparison of all data sets with the elastoplastic constriction model

Data Set	Flow stress S_f MPa	% maximum error $\psi = (1-a/b)^{1.5}$	% RMS error $\psi = (1-a/b)^{1.5}$	% RMS error $\psi = 1.0$
F1 (Indenter1-Flat1)	206	4.2	2.4	5.8
F2 (Indenter2-Flat2)	194	8.3	5.5	4.2
F3 (Indenter2-Flat3)	NR	-8.5	6.1	7.3
F4 (Indenter2-Flat4)	NR	-7.0	3.1	5.5
K1 (Indenter3-Flat5)	NR	-6.4	3.9	5.9

*NR = Not Required (Use $S_f = \infty$ in Eq. (8))

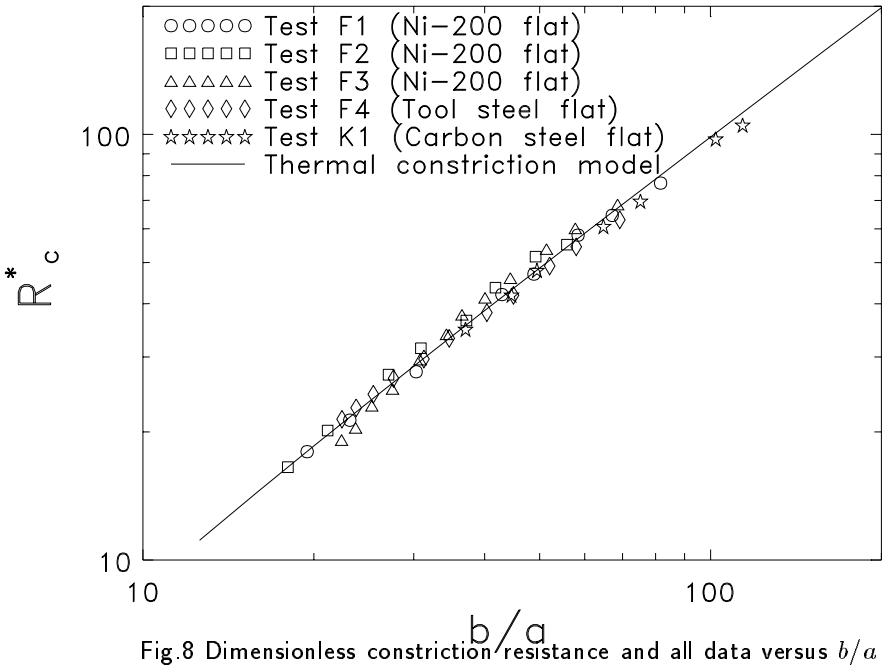

Fig.8 Dimensionless constriction resistance and all data versus b/a

Figure 8 shows a comparison between the proposed elastoplastic constriction model and all data for a plot of dimensionless constriction resistance R_c^* versus the parameter b/a which is inversely related to the applied load F. The model is independent of the type of deformation and is a plot of Eq. (16). Whereas b/a for the data sets had to be calculated using the elastoplastic deformation model. In Fig. 8 the lighest load data points can be seen at the top end and the highest load data at the lower end. The model appears non-linear (log-log scale) at the lower end. This is due to the effect of the thermal constriction parameter ψ.

The advantage of defining a dimensionless constriction resistance can be seen in Fig. 8. Irrespective of the type of deformation, thermophysical properties, geometries and materials used, all data sets can be plotted on one graph. The experimental data include i) Fisher (1985) sets F1 and F2 where deformation is elastoplastic, ii) Fisher (1985) and Fisher and Yovanovich (1989) sets F3 and F4 where deformation is fully elastic and iii) Kitscha (1982) set K1 where deformation is fully elastic. It is seen that the data points lie close to the model, they fall on either side, and the comparison is very good with an overall RMS error of 4.5 %.

SUMMARY AND CONCLUSIONS

The thermal constriction resistance model in conjunction with the elastoplastic deformation model is very versatile and can predict experimental results in any deformation regime with good accuracy.

The use of the thermal constriction parameter in the thermal constriction resistance model enhances its ability to predict the experimental results at high loads.

The problem of not using an appropriate value of flow stress in the elastoplastic deformation model has been addressed here and the proposed technique to compute the flow stress seems to work quite well with the experimental data sets. In future it is suggested that an uniaxial tensile test be performed on the softer material in contact so that the appropriate value of flow stress can be obtained from it and used in the elastoplastic deformation model.

ACKNOWLEDGMENTS

The authors acknowledge the support of the Natural Science and Engineering Research Council of Canada under grant A7445.

REFERENCES

Archard, J.F., 1980, Wear Theory and Mechanisms, *Wear Control Hand-book*, M.B. Peterson and W.O. Winer, eds., ASME, New York, pp. 35-80.

Bar-Cohen, A., 1987, "Packaging and Physical Modelling Trends in the Electronics Industry," Presented at the 1st UTK/ECN SIG on Packaging and Physical Modelling of Electronic Systems, University of Tennessee, Knoxville, Tennessee.

Cooper, M. G., Mikic, B. B., and Yovanovich M. M., 1969, "Thermal Contact Conductance," *Int. J. Heat Mass Transfer*, Vol. 12, pp. 279-300.

Fisher, N.J., 1985, "Analytical and Experimental Studies of the Thermal Contact Resistance of Sphere/Layered Flat Contacts," M.A.Sc. Thesis, University of Waterloo, Canada.

Fisher, N. J., and Yovanovich, M. M., 1989, "Thermal Constriction Resistance of Sphere/Layered Flat Contacts: Theory and Experiment," ASME, *Journal of Heat Transfer,* Vol. 111, pp. 249-256.

Hertz, H. R., 1896, *Miscellaneous Papers.*, English Translation., Macmillan and Co., London.

Johnson, K. L., 1985, *Contact Mechanics*, Cambridge University Press, Cambridge, Cambridge.

Kitscha, W., 1982, "Thermal Resistance of Sphere-Flat Contacts," M.A.Sc. Thesis, University of Waterloo, Canada.

Sridhar, M. R., and Yovanovich M. M., 1993, "Elastoplastic Model for Indentation of Annealed to Fully Work-Hardened Half-Spaces by an Frictionless Elastic Sphere," paper under preparation.

Tabor, D., 1951, *The Hardness of Metals*, Oxford University Press, London.

Wolfram, S., 1988, 1991, *A System for Doing Mathematics by Computer*, Version 2.0 for DOS, Wolfram Research, Inc., Champaign, Illinois.